AIAA JOURNAL
Vol. 40, No. 8, August 2002

Static Shape Control of Composite Plates Using a Slope-Displacement-Based Algorithm

Clinton Y. K. Chee,* Liyong Tong,† and Grant P. Steven‡
University of Sydney, Sydney, New South Wales 2006, Australia

An intuitive approach for the determination of voltage distribution in the application to shape control of smart structures using piezoelectric actuators is presented. This novel approach introduces slope as the fine-tuning criterion on top of the common displacement-based shape control. The algorithm, called the perturbation buildup voltage distribution is based on an iterative approach inspired by a previous algorithm on displacement control. This method aims to provide a means of targeting the desired shape of a structure with a higher-order criterion such as slope. A natural consequence of this method is the smoothing of the resultant structure. This effect will be illustrated by numerical examples. Iterative parameters are varied to investigate favorable choices of the parameters. Results show that the slopes of the structure can be improved, but at a tolerable expense of the displacement criteria. Another result of practical interest is the reduction of internal stresses compared to cases using pure displacement shape control.

Introduction

OVER the past decade, significant interest has been raised in the field of smart or intelligent structures. Until recently, structural engineering usually involved structures that are passive, but the new technology of smart structures involves active structures, that is, structures with the ability to change their overall properties or configuration while in operation. The smartness or the intelligence of the structure refers to the ability of the structure to actuate itself based on some built-in control algorithm, to actuate the adaptive materials incorporated in the structure depending on the response obtained by a set of sensors also made of adaptive materials. Such a self-contained system has the ability to perform various tasks such as vibration control, shape control, health monitoring, and stability control.

The field of shape control has been in existence since before that of smart structures, in particular regarding the shape control of space antenna, reflectors, etc.[1] Much of this work involving space truss structures was based on controlling the shape at discrete points using conventional axial (point) actuators. The application considered in this paper is that of quasi-static shape control. Shape control involves activating the structure to achieve a certain desired shape specified by the user. Applications range from controlling the shape of aerodynamic surfaces, such as an airfoil, large flexible space structures,[2] or space antenna reflectors.[3] It has been noted that smart actuators integrated within the structure produce small in-plane deflections that can, in turn, produce large out-of-plane deformations.[4] The objectives of shape control include determining the magnitude of input signal to apply to each actuator, or the optimal layout of actuators, as well as determining any other variables that might affect the behavior of the structure, to obtain a shape that is as close as possible to the desired shape. Several works presented results of various shapes obtained by changing input parameters such as actuator size, location, and actuator voltages.[5,6] Although the viability of the shape control of structures was shown, the shape control problem was not addressed directly.

The true shape control problem is a type of inverse problem with no explicit solutions. The core of shape control is to minimize the cost functional, usually defined as the squared difference of displacements between the desired and the calculated/actual shape.[7–9] Koconis et al.[7,8] developed analytical methods for composite plates and shells based on sandwich structures and finding solutions to expressions corresponding to zero slope with respect to variables to be optimized. Hsu et al.[9] adopted finite elements for composite plates and used a gradient projection method to find the search direction. Until now, most plate models have been based on Kirchhoff's thin-plate theory or the first-order shear deformation theory; there has been little work on shape control using high-order displacement theories for composite plates.

An iterative approach for shape control of composite beams was formulated by Chandrashekhara and Varadarajan[10] using Reddy's[11] third-order displacement theory, whereas the composite plate version[12] used first-order shear deformation theory. In addition to minimizing the error function, they also considered closed-loop control where the displacements are fed back to determine the next set of input voltages. Techniques of using optimal linear quadratic Gaussian for shape control of smart structures were implemented by Balakrishnan[13] and Tan and Bainum.[14,15] Alternatively, there are simpler heuristic methods that have been developed for general shape control of structures that are not necessarily smart structures. Some of these are the worst-in–best-out, the exhaustive single point substitution,[1] and Skelton and DeLorenzo's (SD) method (see Ref. 1). The latter algorithm is based on choosing all actuators initially and then removing those that make the least contribution. Another method, called the successive peak error correction (SPEC)[16] was declared to be faster than the SD method but with comparable precision.

The present work will consider a composite laminate plate structure as the smart structure, using piezoelectric materials as the adaptive actuators. The mathematical model is a hybrid of a high- (third-) order displacement theory and layerwise concept[17] that fully accounts for the electromechanical coupling. This also allows both thin and thick composite structures to be modeled, and the piezoelectric actuators can be placed in any of the layers, that is, embedded or surface bonded. The model is then incorporated into a finite element (FE) formulation that, in general, also accommodates greater freedom as to where the actuators may be placed. The use of finite element analysis (FEA) means that the geometry is not restricted to simple shapes, unlike that required by exact analytical solution methodologies. The FEA calculations will be done using an in-house developed program based on the theoretical formulation.

Received 17 March 2000; revision received 25 May 2001; accepted for publication 8 February 2002.

*Research Engineer, Composite and Smart Structures Group, Department of Aeronautical Engineering; aerochee@lycos.com. Member AIAA.

†Associate Professor, Composite and Smart Structures Group, Department of Aeronautical Engineering, Building J07; ltong@aero.usyd.edu.au. Member AIAA.

‡Lawrence Hargrave Professor of Aeronautical Engineering, Composite and Smart Structures Group, Head of Department.

In Ref. 18, an intuitive/heuristic shape control algorithm was developed that has been inspired by elements of the SPEC method, evolutionary strategies, and artificial neural networks. The algorithm, called buildup voltage distribution (BVD), iteratively builds up the voltage magnitudes of each potentially active patch, thus resulting in a final voltage distribution.

Like many other shape control methods, BVD is solely displacement based. The new contribution of the present work is to introduce slope as the next criterion for shape control. This algorithm, called perturbation buildup voltage distribution (PBVD), is an iterative algorithm with a concept similar to BVD. Initially, displacement shape control based on a linear least-square (LLS) fit is performed on the structure. The result is a structure with some bumpiness, and this is taken as the initial configuration for PBVD. In PBVD, slope is regarded as the fine-tuning criterion used to smoothen the structure. In the iterative process, the voltages are perturbed and build up based on a cost function determined by the slope.

Unlike the least-squares method, PBVD makes no assumption on linearity and, hence, can be used for general nonlinear piezoelastic systems. Initial investigation include dual criteria displacement-slope shape control using LLS. It will be shown that these two effects are competing, and that PBVD was developed to smoothen the structure using slope criterion, but at a tolerable expense of the displacement criterion.

Mathematical Model

The theoretical formulation combines the high-order displacement (HOD) field and a linear layerwise voltage field. They will be incorporated into the FE formulation with displacements and voltages as the nodal variables. A more detailed development of the mathematical model can be found in Ref. 17.

Governing Equations

The mechanical behavior of the structure is modeled by the third-order displacement field, used by Lo et al.,[19] as shown in Eq. (1):

$$U(x, y, z) = u_0(x, y) + z\psi_x(x, y) + z^2\zeta_x(x, y) + z^3\varphi_x(x, y)$$

$$V(x, y, z) = v_0(x, y) + z\psi_y(x, y) + z^2\zeta_y(x, y) + z^3\varphi_y(x, y)$$

$$W(x, y, z) = w_0(x, y) + z\psi_z(x, y) + z^2\zeta_z(x, y) \tag{1}$$

The displacement functions U, V, and W in the x, y, and z directions are composed of in-plane subfunctions such as $u_0(x, y)$, $v_0(x, y)$, $\psi_x(x, y)$, etc., which are separated from the thickness z dimension. The advantages of the cubic HOD are 1) that it is suitable for both thick and thin composite structures, 2) that no shear correction factor is required, 3) that it models the transverse shear effects and captures a parabolic transverse shear strain across the thickness of the structure, 4) that transverse normal strain is also accounted for, 5) that there is less restriction on the type of problem because displacement field is independent of boundary conditions and material properties, and 6) that the absence of derivatives in the displacement field means that C^0 shape functions can be used in the FE formulation. This represents a total of 11 mechanical degrees of freedom:

$$u = [u_0 \quad v_0 \quad w_0 \quad \psi_x \quad \psi_y \quad \psi_z \quad \zeta_x \quad \zeta_y \quad \zeta_z \quad \varphi_x \quad \varphi_y]^T \tag{2}$$

The strain vectors in Eq. (3) are defined in the usual manner and, thus, will not be elaborated on further:

$$[\varepsilon_1 \quad \varepsilon_2 \quad \varepsilon_3 \quad \varepsilon_6]^T = \varepsilon_b = D_b u$$

$$[\varepsilon_4 \quad \varepsilon_5]^T = \varepsilon_s = D_s u \tag{3}$$

The linear layerwise formulation has been used by Saravanos and Heyliger[20] and before them, Robbins and Reddy.[21] This technique will be applied to the electric potential and separates the field into planar φ_j and transverse layerwise L_j functions. A general layerwise function may be written as in Eq. (4):

$$\Phi(x, y, z, t) = \sum_{j=1}^{n\,\text{layers}+1} L_j(z)\varphi_j(x, y, t) \tag{4}$$

The structure or laminate is divided into several layers, and each layer can be approximated by a linear electric potential field in the z direction. Hence, if the overall electric potential across the thickness is a polynomial function of n degrees, then there should be at least n discrete layers for this layerwise approximation. Thus, the electric potential within the kth layer is given in Eq. (5):

$$\Phi(x, y, z)_k = L_{kd}(z)\varphi_k(x, y) + L_{ku}(z)\varphi_{k+1}(x, y) \tag{5a}$$

where

$$L_{kd}(z) = \frac{z - z_{k+1}}{z_k - z_{k+1}}, \qquad L_{ku}(z) = \frac{z - z_k}{z_{k+1} - z_k} \tag{5b}$$

Note that $\varphi_k(x, y)$ and $\varphi_{k+1}(x, y)$, are functions at the kth and $(k+1)$th interfaces, respectively.

From the definition of the electric field as the negative gradient of the electric potential, the layerwise expression for the electric field at the kth layer is

$$\begin{bmatrix} E_x(x, y, z) \\ E_y(x, y, z) \\ E_z(x, y, z) \end{bmatrix}_k = -\begin{bmatrix} L_{kd}(z)\dfrac{\partial\varphi_k(x, y)}{\partial x} + L_{ku}(z)\dfrac{\partial\varphi_{k+1}(x, y)}{\partial x} \\ L_{kd}(z)\dfrac{\partial\varphi_k(x, y)}{\partial y} + L_{ku}(z)\dfrac{\partial\varphi_{k+1}(x, y)}{\partial y} \\ \dfrac{1}{z_k - z_{k+1}}\varphi_k(x, y) + \dfrac{1}{z_{k+1} - z_k}\varphi_{k+1}(x, y) \end{bmatrix} \tag{6}$$

The FE formulation is based on the Hamilton's variational principle, which considers the strain potential energy and work for the whole structure. Thus, the mechanical behavior modeled by the HOD theory and the electrical behavior modeled by the layerwise theory will be fully coupled. The natural boundary conditions are also implicitly accounted for. The present work will neglect the kinetic energy term.

The potential energy is the internal potential strain energy of the system or structure. For piezoelectric systems (i.e., structures that have parts that are piezoelectric materials), the potential energy[22] is

$$\mathrm{d}P = (\sigma\,\mathrm{d}\varepsilon - D\,\mathrm{d}E) \times \text{volume} \tag{7}$$

The specific form of potential energy P of Eq. (7) is chosen because its natural variables are strain ε and electric field E, both of which can be expressed in terms of displacement and electric voltage, respectively, which are obvious choices as degrees of freedom in FEA. This necessitates the use of the stress formulation of the piezoelectric constitutive equation as shown in Eq. (8):

$$\begin{pmatrix} \sigma_1 \\ \sigma_2 \\ \sigma_3 \\ \sigma_6 \end{pmatrix} = \begin{bmatrix} c_{11} & c_{12} & c_{13} & c_{16} \\ c_{12} & c_{22} & c_{23} & c_{26} \\ c_{13} & c_{23} & c_{33} & c_{36} \\ c_{16} & c_{26} & c_{36} & c_{66} \end{bmatrix} \begin{pmatrix} \varepsilon_1 \\ \varepsilon_2 \\ \varepsilon_3 \\ \varepsilon_6 \end{pmatrix} - \begin{pmatrix} e_{31} \\ e_{32} \\ e_{33} \\ e_{36} \end{pmatrix} E_3$$

$$\sigma_b = c_b\varepsilon_b - e_b^T E_0$$

$$\begin{pmatrix} \sigma_4 \\ \sigma_5 \end{pmatrix} = \begin{bmatrix} c_{44} & c_{45} \\ c_{45} & c_{55} \end{bmatrix} \begin{pmatrix} \varepsilon_4 \\ \varepsilon_5 \end{pmatrix} - \begin{bmatrix} e_{14} & e_{24} \\ e_{15} & e_{14} \end{bmatrix} \begin{pmatrix} E_1 \\ E_2 \end{pmatrix}$$

$$\sigma_s = c_s\varepsilon_s - e_s^T E_i \tag{8a}$$

$$\begin{pmatrix} D_1 \\ D_2 \end{pmatrix} = \begin{bmatrix} e_{14} & e_{15} \\ e_{24} & e_{14} \end{bmatrix} \begin{pmatrix} \varepsilon_4 \\ \varepsilon_5 \end{pmatrix} + \begin{bmatrix} \chi_{11} & \chi_{12} \\ \chi_{12} & \chi_{22} \end{bmatrix} \begin{pmatrix} E_1 \\ E_2 \end{pmatrix}$$

$$D_i = e_s\varepsilon_s + \chi_i E_i$$

$$D_3 = [e_{31} \quad e_{32} \quad e_{33} \quad e_{36}]\varepsilon_b + \chi_{33}E_3$$

$$D_0 = e_b\varepsilon_b + \chi_0 E_0 \tag{8b}$$

The substrate material is orthotropic at most, and the piezoelectric material is orthorhombic, class mm2 as indicated by Eq. (8). Piezoelectric stress coefficients (e_b and e_s) are set to zero for nonpiezoelectric materials. The global coordinate system used in Eq. (8) has taken into account the rotation of the material about the transverse normal z axis. For a material with zero rotation, the following material coefficients are zero: c_{16}, c_{26}, c_{36}, c_{45}, e_{14}, e_{36}, and χ_{12}.

By the use of the constitutive Eqs. (8), the potential energy integral can be expressed in terms of virtual strains and electric fields as

$$\delta \int_{t_1}^{t_2} P \, \mathrm{d}t = \int_{t_1}^{t_2} \int_V \left\{ \delta \varepsilon_b^T \left(c_b \varepsilon_b - e_b^T E_0 \right) + \delta \varepsilon_s^T \left(c_s \varepsilon_s - e_s^T E_i \right) - \delta E_i^T (e_s \varepsilon_s + \chi_i E_i) - \delta E_0^T (e_b \varepsilon_b + \chi_0 E_0) \right\} \mathrm{d}V \, \mathrm{d}t \tag{9a}$$

The virtual work due to the externally applied load is the product of the variational generalized coordinates and the virtual forces. Thus, in general, the total virtual work δW of a structure is due to the mechanical forces including volume forces $\boldsymbol{F}^V$, surface forces $\boldsymbol{F}^S$, and point forces $\boldsymbol{F}^P$ acting on displacements $\boldsymbol{U}_T$. They are also due to electrical surface charges Q^S in the presence of an electric potential difference ϕ. Thus, the integral of the variation of work is given in Eq. (9b) in terms of force vectors, displacement vectors, surface charge, and electric potential:

$$\int_{t_0}^{t_1} \delta W \, \mathrm{d}t = \int_{t_0}^{t_1} \left(\int_V \delta U_T^T F^V \, \mathrm{d}V + \int_S \delta U_T^T F^S \, \mathrm{d}S + \delta U_T^T F^P - \int_S \delta \varphi Q^S \, \mathrm{d}S \right) \mathrm{d}t \tag{9b}$$

To achieve practical solutions from the analytical formulation described, an FE formulation with electric potential and mechanical variables as the degrees of freedom is introduced. In the present work, an eight-node HOD-layerwise rectangular plate element has been developed. Although the FE implementation shown hereafter appears standard, there is novelty in the specific form of the combination of the HOD-layerwise concept.

The real displacement functions [Eq. (1)] and strains [Eq. (3)] in terms of the nodal variables $[u_e]$ are given in Eqs. (10) and (11):

$$\begin{bmatrix} U(x, y, z) \\ V(x, y, z) \\ W(x, y, z) \end{bmatrix} = [A(z)][N_u(\xi, \eta)][u_e] \tag{10}$$

$$[\varepsilon_b(x, y, z)] = [D_b(x, y, z)][N_u(\xi, \eta)][u_e]$$

$$[\varepsilon_s(x, y, z)] = [D_s(x, y, z)][N_u(\xi, \eta)][u_e] \tag{11}$$

The shape function matrix $N_u(\xi, \eta)$ in Eq. (10) is an $11 \times (11 \times 8)$ matrix that uses the standard eight node serendipitous shape functions. The electric counterpart of the shape function matrix is $N_\varphi(\xi, \eta, z)_k$, with dimension $1 \times 8(n+1)$, and it incorporates the layerwise and the eight-node shape functions. It relates the nodal voltages to the voltage function [Eq. (12)] of the eth element at the kth layer and the electric field:

$$\Phi(x, y, z)_k^e = [N_\varphi(\xi, \eta, z)_k][\varphi_e] \tag{12}$$

$$[E(x, y, z)]_k^e = -\nabla [N_\varphi(\xi, \eta, z)_k][\varphi_e] \tag{13}$$

Finally, by application of the variational principle by including the definitions of Eqs. (10–13), the governing equation of the structure in terms of the FE nodal variables is obtained in Eq. (14):

$$\begin{bmatrix} [K_{uu}] & [K_{u\varphi}] \\ [K_{\varphi u}] & [K_{\varphi\varphi}] \end{bmatrix} \begin{bmatrix} u_g \\ \varphi_g \end{bmatrix} = \begin{bmatrix} [F_g] \\ -[Q_g] \end{bmatrix} \tag{14}$$

Equation (14) represents the summation of the equations of all of the elements and, thus, is the global equation for the system, hence the subscripts g. The mechanical, electrical, and electromechanically coupled stiffness of the structure are represented on the leftside of Eq. (14), whereas the externally applied forces F_g and externally applied charges Q_g are represented on the right-hand side of Eq. (14). This formulation is general in the sense that it can model laminated composite structures with arbitrary boundary conditions. The robustness of this formulation is that each element of each layer can be made of any material, and if it is piezoelectric, then setting the appropriate (electrical) boundary conditions will allow it to act as an actuator or sensor.

PBVD Shape Control

Many existing shape control algorithms are formulated from displacement-based cost functions. Chee et al.[18] showed that simple desired shape and configuration can be obtain with relative ease, whereas more complex desired shapes or structural configurations are achievable globally, but introduce some uneveness locally. An example of a structure obtained by simple LLS fit superimposed on its desired shape is shown in Fig. 1 (details found in the "Numerical Examples" section). Note the resultant bumpiness of the structure. Preliminary investigations using dual criteria slope-displacement LLS shape control resulted in Fig. 2. The middle part of the structure appeared to be have been smoothed, but tip displacements are worse than in the pure displacement-shape control case.

A possible improvement in dual criteria LLS is to assign weights to the slope and displacements. However, the determination of weights would not be a trivial task. Thus, an iterative perturbation technique is introduced, and it implicitly targets regions that need the most improvement. The PBVD concentrates on iteratively correcting the slopes locally. A consequence of PBVD will be the smoothing of the actual structure because the slope is being controlled. This is achieved without significant sacrifice of the target displacement. Although the name and concept of the algorithm is motivated by BVD[18] (a purely displacement-based shape control), the PBVD algorithm is significantly different.

Defining the Problem

The structure whose shape is to be controlled is a laminated composite plate in/on which piezoelectric actuators can be embedded or surface attached. The electric field is applied in the normal direction of the composite plane. The actuators are discretized as patches to distinguish them from the hypothetical, computational elements in

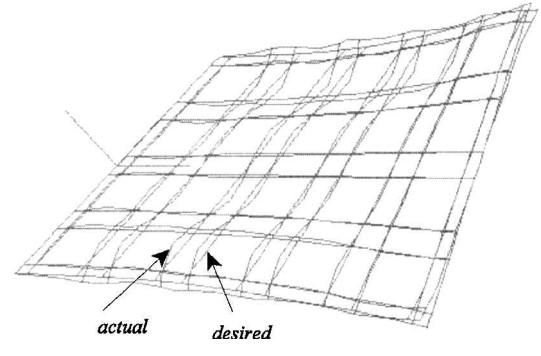

Fig. 1 Midplane transverse displacement of cantilever plate with a twisted desired shape; actual shape by displacement LLS is superimposed (oblique view).

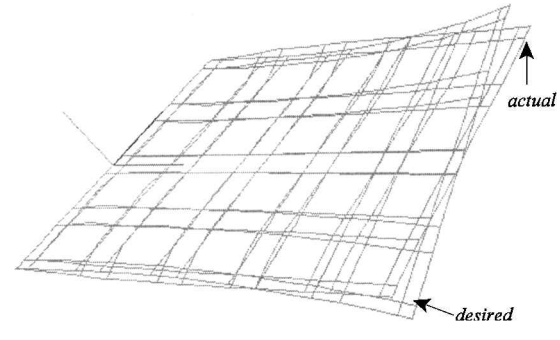

Fig. 2 Dual criteria slope and displacement shape control using LLS.

FE analysis. Thus, for the FE analysis, a patch is constructed of at least one element. The size of the patch is the real size of the actuator, whereas the size of the element is determined by the user, depending on the structural topology and desired accuracy of the FE mesh.

Electrical voltages are imposed as boundary conditions such that the top and bottom surfaces of each patch have constant voltages. The implementation of this condition in the FEA is achieved by assigning the same voltage values to all nodes of each actuator patch surface at each interface. Thus, the nodal voltage vector ϕ_e of Eq. (12) would be a constant vector, whereas in Eq. (5) each voltage interface function would be a constant value.

The shape control problem analyzed in this paper involves finding the voltage distribution, that is, the magnitude of voltages to be applied to each of the piezoelectric patches. The desired shape of the structure is known, either as a mathematical function or as the specification of the displacements at the nodes. There exists a linear relationship between the voltage and displacement[18] and, hence, also between the voltage and slope, due to the linear model of the constitutive properties and the governing equations. Thus, the slopes (for the eth element) and transverse nodal displacements (for the whole structure) can be directly related to the applied patch voltages [Eq. (15–16)] by the influence coefficient matrices obtained by FEA:

$$\{w\} = [C_w]\{\varphi\} = \sum_{k=1}^{Np} \{C_w\}_k \varphi_k = \{C_w\}_1 \varphi_1 + \{C_w\}_2 \varphi_2 + \cdots + \{C_w\}_{Np} \varphi_{Np} \tag{15}$$

$$\{S_x\} = [C_{sx}]\{\varphi\} = \sum_{k=1}^{Np} \{C_{sx}\}_k \varphi_k \tag{16}$$

where $S_x = \partial w/\partial x$, C_{sx} is the matrix of coefficient of S_x, ϕ_k is the voltage on patch k, and N_p is the number of active patches.

When the voltage is perturbed by a small amount $\mathrm{d}\phi_k$ at patch k only, from the base voltage configuration $\{\phi^0\}$ then the slopes of the perturbed structure are given by Eq. (17), where superscript 0 represents the quantities in base configuration:

$$\{S_x\} = \left\{S_x^0\right\} + \{C_{sx}\}_k \,\mathrm{d}\varphi_k \tag{17}$$

PBVD Algorithm

The PBVD method starts with the initial configuration, which is the resultant of pure displacement shape control using LLS. The strategy involves improving the slope of the structure on an elemental basis, where the elements with larger slope discrepancies (compared to the desired slope values) will be improved first. The voltage required to improve the slope in an element will be calculated such that only small improvements are made at each iteration, hence, requiring only small amounts of incremental voltage at a time.

The measure of transverse displacements is the sum of the squared difference w_Δ between the desired and the actual nodal values. However, the slopes are measured on an elemental basis. Hence, the area integral of the squared difference $S_{x\Delta}$ of the desired and actual slope is used. This has the advantage of placing more importance on the improvement of slopes of larger-sized elements.

To investigate the voltage perturbation effect on the slope, the new slope is compared with the original slope with respect to the desired slope. Because the displacement and slope are, in fact, competing criteria, the improvement of the slope of the structure will be at the expense of achieving the desired displacement. When a tolerance factor p is incorporated, it is possible to aim for an improvement in the slope, at the same time restricting the displacement criteria from deteriorating excessively. This dual criteria is expressed in Eq. (18):

$$\int_A \left(S_x^e - S_x^{e^d}\right)^2 \mathrm{d}A_e < (1-p) \int_A \left(S_x^{e^0} - S_x^{e^d}\right)^2 \mathrm{d}A_e$$

$$\sum_{i=1}^{\text{nodes}} \left(w_i - w_i^d\right)^2 < (1+p) \sum_{1}^{\text{nodes}} \left(w_i^0 - w_i^d\right)^2 \tag{18}$$

where superscript d represents desired quantities. Note that the equation involving S_y would be similar to Eq. (18).

During each iteration, an incremental voltage will be added temporarily, and the effects on the slope of the other elements as well as displacements are checked. If the side effects of adding $\mathrm{d}\phi$ are tolerable, then it is added permanently, and the new voltage configuration will be used in the next iteration.

Perturbing the voltage at the kth patch only, the dual criteria are reexpressed as in Eq. (19):

$$p \int \left(S_x^{e'}\right)^2 \mathrm{d}A + 2\,\mathrm{d}\varphi \int \left(S_x^{e'}\right)\left(C_{sx}^e\right)_k \mathrm{d}A + \mathrm{d}\varphi^2 \int \left(C_{sx}^e\right)_k^2 \mathrm{d}A < 0$$

$$-p \sum_{i=1}^{\text{nodes}} (w_i')^2 + 2\,\mathrm{d}\varphi \sum_{i=1}^{\text{nodes}} w_i' \left(C_w^e\right)_{ki} + \mathrm{d}\varphi^2 \sum_{i=1}^{\text{nodes}} \left(C_w^e\right)_{ki}^2 < 0 \tag{19}$$

and enable the calculation of the optimum incremental voltage $\mathrm{d}\phi$, where $S_x^{e'} = S_x^{eo} + S_x^{ed}$ and $w' = w^0 + w^d$.

Another quantity that is used later is the patch sensitivity index (PI), which is defined in Eq. (20):

$$\mathrm{PI}^{sx}(k, e) = \frac{\varphi_k - \varphi_k^0}{S_{x\Delta} - S_{x\Delta}^0}, \qquad \varphi_k = \varphi_k^0 + 1$$

$$\mathrm{PI}^{sx}(k, e) = \frac{1}{\int_A C_{sxk}^e \left(\varphi_k^0 + 1\right)\left[C_{sxk}^e \left(\varphi_k^0 + 1\right) + 2S_x^{e'}\right] \mathrm{d}A_e} \tag{20}$$

Large $\mathrm{PI}(k, e)$ values imply that element e is insensitive to the voltage applied to patch k.

The PBVD algorithm is summarized as follows:

1) Perform displacement shape control using LLS, and use the resultant voltage configuration as the initial configuration for PBVD.

2) Calculate w_Δ and $(S_{x\Delta}^e)$, $(S_{y\Delta}^e)$ for all elements e.

3) Sort the $(S_{x\Delta}^e)$, $(S_{y\Delta}^e)$ from the highest magnitude to the lowest.

4) Select an element with high (S_Δ^e) to be improved on. A normal probability distribution selection mechanism is used so that elements with higher (but not necessarily the highest) (S_Δ^e) magnitude are more likely to be selected.

5) Calculate $\mathrm{PI}^{sx}(k, e)$ and $\mathrm{PI}^{sy}(k, e)$ for the kth patch and the eth element for all patches and all elements.

6) Sort the slope sensitivities among all patches, for the selected element.

7) Begin iteration of voltage perturbation starting from the most sensitive patch.

8) Calculate incremental voltage $\mathrm{d}\phi$ necessary to improve slope for this element, but with a tolerable worsening in displacement. This is done by finding the optimum $\mathrm{d}\phi$ of Eq. (19).

9) Apply $\mathrm{d}\phi$ and recalculate w_Δ and $(S_{x\Delta}^e)$, $(S_{y\Delta}^e)$ for all elements.

10) Check for adverse effects in the slopes of other elements when $\mathrm{d}\phi$ was applied to patch k. If the slope of the other elements are within a tolerable limit, then accept the new voltage configuration and begin the next iteration in step 2. Otherwise, go to step 7 to perturb the next patch.

11) Continue iteration until the maximum number of iterations is reached or the tolerance on the original w_Δ is exceeded.

Numerical Examples

Test Model Description

The structural model for the following set of tests is depicted in Fig. 3. The 20 shaded regions represent areas designated as active patches. For the FEA, the structure is divided into 99 elements. In the present case, each patch is modeled by one FE. The dimensions of the cantilever plate are length $L = 0.150$ m and width $C = 0.120$ m. The thickness of the single-layered substrate is $2.0e{-}3$ m. The gap between the patches and the edge is 0.005 m, and the gap between the patches themselves is 0.010 m. The aluminum substrate has the following stiffnesses: $c_{11} = c_{22} = c_{33} = 105.896$, $c_{12} = c_{23} = c_{13} = 54.552$, and $c_{44} = c_{55} = c_{66} = 25.67$ GPa. The piezoelectric actuators (PIC151), with thickness of $5.0e{-}4$ m, are located at the regions corresponding to the patches and are attached to the top and bottom layer of the substrate. Their properties are stiffness $c_{11} = c_{22} = 107.6$, $c_{33} = 100.4$, $c_{12} = 63.12$,

Table 1 Percentage improvement of slope and displacement measure after applying PBVD

Parameter[a]	Case 1	Case 2	Case 3	Case 4
LSd.tol	0.05	0.5	5.5	5.5
Mult. Iter	1.9	1.9	100.9	100.9
p.tol	0.001	0.01	0.01	0.1
s.tol	0.3	0.3	2.3	30.03
w-disp	5.0267%	50.2868%	88.0973%	176.8081%
slope_x	−3.8311%	−1.7371%	3.4044%	14.9528%
slope_y	−7.1609%	−22.2148%	−29.2904%	−49.1477%

[a]Explained in text.

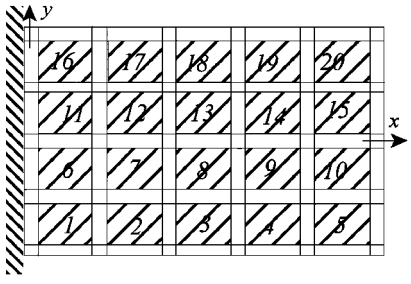

Fig. 3 Cantilever plate with 99 elements and 20 active patches (not to scale).

$c_{23} = c_{13} = 63.85$, $c_{44} = c_{55} = 19.62$, and $c_{66} = 22.24$ GPa; electric permittivity $\chi_{11} = \chi_{22} = 9.818$ and $\chi_{33} = 7.536$ nF/m; and piezoelectric strain constants $d_{31} = d_{32} = -214.0$, $d_{33} = 423.0$, and $d_{15} = d_{24} = 610.0$ pm/V. No external mechanical forces ($F_g = 0$) and no external electric charges ($Q_g = 0$) will be applied to this structure.

The present study focuses in obtaining a twisted desired shape because this is the interesting case where PBVD is needed to improve the structure after the initial displacement shape control stage. The desired shape is specified by Eq. (21), where G is the scaling factor, in this case $G = 1$. The twisted, wide cantilever example may represent a wing structure that is required to be twisted for aerodynamic purposes:

$$w(x, y) = [\cosh(x) - 1]\sin(y)/G \tag{21}$$

Performance of Slope-Based Shape Control

Preliminary investigation of this structure using a purely displacement LLS method for shape control resulted in the structure in Fig. 1. This suggests that although the nodal displacements may have matched well, the LLS method contains no mechanism that monitors the slope of the structure. Hence, the overall twisting effect was achieved, but there are regions of bumpiness. In the next stage, the slopes were incorporated into the LLS, and this simultaneous dual criteria (slope-displacement) shape control resulted in Fig. 2. Significant improvement is evident as the center of the structure is smoothed, but the tip displacements worsened. Improvements could be made by making use of weights, but therein lies the disadvantage of having to choose the weights arbitrarily. Although the results are not shown here, note that different weights on displacement and slope have little effect on the results using LLS.

PBVD is a less rigid alternative to LLS that incorporates an element of randomness in the iterative process and does not require weights. Instead, it allows the user more direct control by specifying various tolerances in the iterative algorithm. Table 1 presents the results of PBVD for four cases with different parameters. The percentage values for w displacement and both slopes in Table 1 represent the percentage differences between the squared difference measure (w_Δ, $S_{x\Delta}$, $S_{y\Delta}$) of the PBVD optimized configuration and their initial purely displacement shape controlled configuration. For this particular case study, it was the slope in the y direction that required more improvement, that is, $S_{x\Delta} < S_{y\Delta}$. This was automatically determined by the algorithm, and the results from Table 1 show the reduction in $S_{y\Delta}$; hence, improvement on the slope in the y direction was achieved. From other data, not published here, the slope in the x direction, in general, was an order of magnitude better than its counterpart and, thus, does not have a high priority for improvement. Table 1 shows that as slope y improves, slope x slightly worsens, but in absolute terms, the slope in the x direction is still better (values not shown here).

Because of the conflicting nature of displacement and slope, when the slope in the y direction improves, the displacement deteriorates, as shown in Table 1. In the first case, when the slope was improved by 7.16%, the displacement worsened by 5.03%. In the last case, when the slope was almost improved by 50%, the displacement deteriorated by 178%. Note that these values are cumulative over the 339 nodal points; hence, the value for each point is, in fact, much lower. Thus, how much improvement in the slope is required and how much deterioration in the displacement criteria is tolerable depend on the specific application. The accuracy of these results depends on the FE software that was integrated with the PBVD, which, in turn, had been validated by Chee et al.[17]

The algorithm has incorporated such tolerance mechanisms as LSdTol, the displacement tolerance above which the PBVD iteration will discontinue; Mult.Iter, a multiplication factor that determines the maximum number of iterations; p.tol, the p factor of Eq. (18) that determines the incremental improvement in slope and the tolerance in displacement for each iteration; and s.tol, the tolerance allowed of the slopes of other elements when the slope of a specific element is improved at each iteration. From Table 1, the iterations of the first two cases were automatically stopped as they exceeded the LsdTol. The s.tol and p.tol influence the speed and the amount of improvement made; a large value would signify a coarse iterative approach that may not yield good solutions. From numerous other tests, favorable results seemed to be obtained when p.tol and s.tol are of the order of magnitude of 0.01 and 1, respectively.

The slope measure $S^e_{y\Delta}$, for each element for the four cases of Table 1, is depicted in Fig. 4 along with the control case (pure displacement control). Clearly, case 4 shows the greatest improvement in slope in the y direction. The three-dimensional view of the

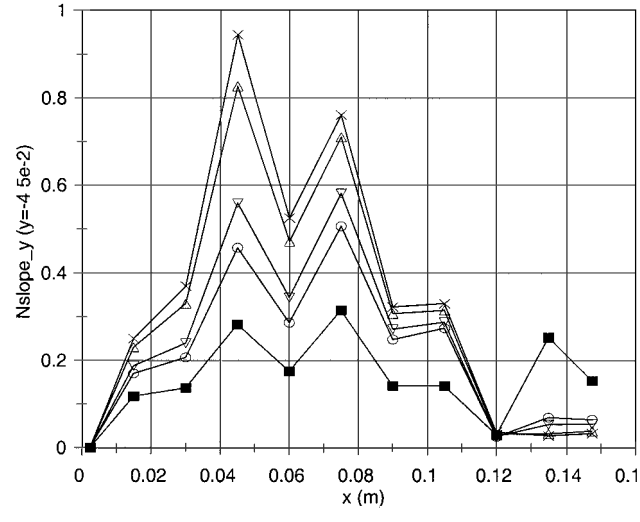

Fig. 4 Normalized slope measure for each element for four PBVD cases and a control case: △, 1; ▽, 2; ○, 3; ■, 4; and ×, ctrl.

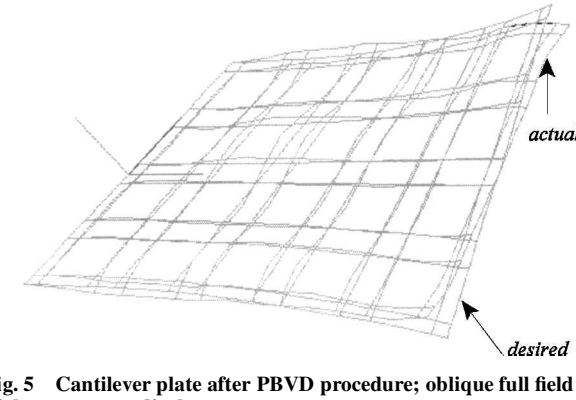

Fig. 5 Cantilever plate after PBVD procedure; oblique full field view of the transverse displacement.

Table 2 Applied voltages of piezoelectric patches predicted by PBVD for slope-displacement shape control vs pure displacement shape control case

Patch number	Pure displacement	Case 1	Case 2	Case 3	Case 4
1	6,023.5	5,997.2	6,023.5	6,023.5	5,437.7
2	12,126.2	11,047.2	8,226.4	7,081.5	4,043.4
3	8,300.9	8,300.9	8,060.7	7,599	6,784.7
4	7,725.5	7,725.5	7,725.5	7,725.5	5,314.1
5	−3,252	−3,252.0	−3,252.0	−3,252.0	−4,590.7
6	8,596	8,512.9	8,596	8,581.9	6,323.7
7	−7,025.2	−7,025.2	−7,025.2	−7,025.2	−3,264.6
8	−3,957.5	−3,957.5	−3,957.5	−3,957.5	−3,957.5
9	−2,832.5	−2,832.5	−2,832.5	−2,832.5	−2,832.5
10	−807.6	−807.6	−807.6	−807.6	−807.6
11	−8,596.0	−8,596.0	−8,596.0	−8,596.0	−7,217.8
12	7,025.2	7,025.2	7,025.2	7,025.2	7,025.2
13	3,957.5	3,957.5	3,957.5	3,957.5	3,957.5
14	2,832.5	2,832.5	2,832.5	2,832.5	1,109.1
15	807.6	807.6	807.6	807.6	807.6
16	−6,023.5	−5,973.5	−6,023.5	−6,023.5	−5,755.5
17	−12,126.2	−10,963.9	−8,258.4	−7,058.5	−5,961.4
18	−8,300.9	−8,300.9	−8,140.3	−7,572.1	−5,974.1
19	−7,725.5	−7,725.5	−7,725.5	−7,725.5	−6,229.2
20	3,252	3,252	3,252	3,252	5,372.5
Total $\|V\|$	121,294	118,893	113,126	109,737	92,767

transverse displacement w at the midplane for case 4 is shown in Fig. 5. Compared with Fig. 1, the regions at the edge of the cantilever plate where the most bumpiness existed have been smoothed. This improvement comes at the expense of the displacement criterion where the tip displacement is noticeably increased.

The voltage configuration predicted by PBVD for the four cases listed in Table 1 are presented in Table 2, along with the voltages for the pure displacement shape control case. The voltages for all cases in Table 2 do seem to be higher than what is currently practical. However, these voltage magnitudes are also an indication of the difficulty of forcing the structure to conform to this particular desired shape [Eq. (21)], given the structural configuration and given the particular choice of materials. For instance, a choice of different materials may ease the voltage requirements to achieve this desired shape. Also, note that the five sets of voltages are different from each other, but some patches have very similar voltages. Looking at the voltage values for case 4, where there is the greatest improvement in the slope in the y direction, the voltage for several patches are lower than the others. In addition, the total magnitude of voltages is the lowest for case 4, implying the lowest electrical energy requirements for this voltage configuration.

Stress Reduction Effect

The existence of complex stress fields within a smart structure should be expected because of the independent localized actuators distributed throughout the structure. In shape control, for the same amount of piezoelectric material incorporated into the structure, better shape controllability is attained by having the piezoelectric material existing as separate patches rather than to have one continuous layer of piezoelectric material across the structure. This is analogous to providing the structure with enough actuation degrees of freedom to achieve a complex shape that can be thought of as a combination of basic shapes. By the imposition of voltages on the actuators, the structure is being coerced into the desired shape. This effect is more forceful in the LLS method because it is a direct approach, whereas the iterative approach of PBVD is more relaxed in its process of calculating the voltage distribution. In either case, when significantly different voltages are applied to various patches, as directed by the shape control algorithm, localized internal stresses are set up. This issue is particularly significant to smart structures, where the actuators are not external, but are regarded as an integral part of the structure.

The bumpiness of the shape of the structure represents, in fact, changes in slope in localized regions. This means that the local curvature has a higher than usual magnitude. In practical terms, this translates to high stresses in certain regions, as well as large variation in stresses between other regions. Because the PBVD algorithm has the ability to smoothen the structure, it can be regarded as a secondary procedure in shape control, used to reduce internal structural stress caused by the primary stage, which is pure displacement-shape control. This conjecture will be validated by the results obtained using the PBVD algorithm.

The following test compares the internal stresses generated within the structure as a result of the pure displacement-shape control using LLS and the stresses obtained after the PBVD procedure is applied. The test model is the same as that described earlier, and for the PBVD case, the set of parameters corresponding to case 4 from Table 1 is used. The voltages of case 4 are also shown in Table 2. The stresses for each element are calculated at their 2×2 Gauss points at a height of $z = 9.0e{-}4$ m, which is within the aluminum substrate. Although all six stresses were calculated, only a selection of the results are presented here due to space limitations. The normal in-plane stresses at $y = -3.923e{-}2$ m along the length of the structure is shown in Fig. 6, with dashed lines for stresses without PBVD and solid lines for stresses with PBVD. There is a clear reduction in the σ_y along the entire length of the structure, and it is mainly tensile stresses. Several points with high σ_x magnitudes were also reduced significantly. Note that this stress is compressive in some regions and tensile in others.

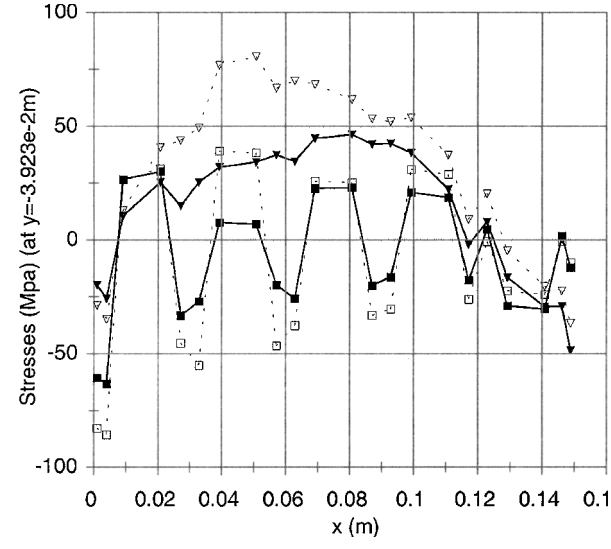

Fig. 6 Reduction of the normal in-plane stresses by the PBVD procedure (y section): ■, str xx; ▼, str yy; □, ostr xx; and ▽, ostr yy.

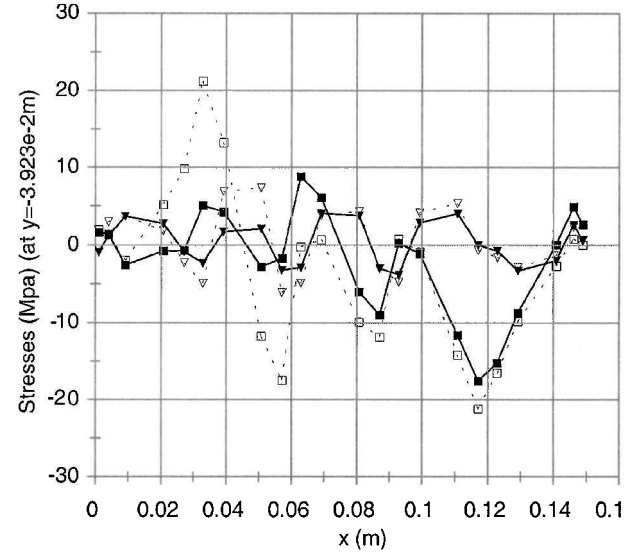

Fig. 7 Reduction of a transverse and in-plane shear by the PBVD procedure (y section): ■, str xy; ▼, str yz; □, ostr xy; and ▽, ostr yz.

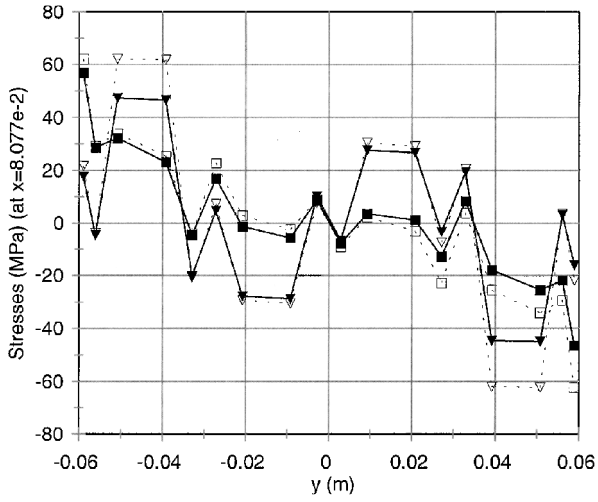

Fig. 8 Reduction of the normal in-plane stresses by the PBVD procedure (x section): ■, str xx; ▼, str yy; □, ostr xx; and ▽, ostr yy.

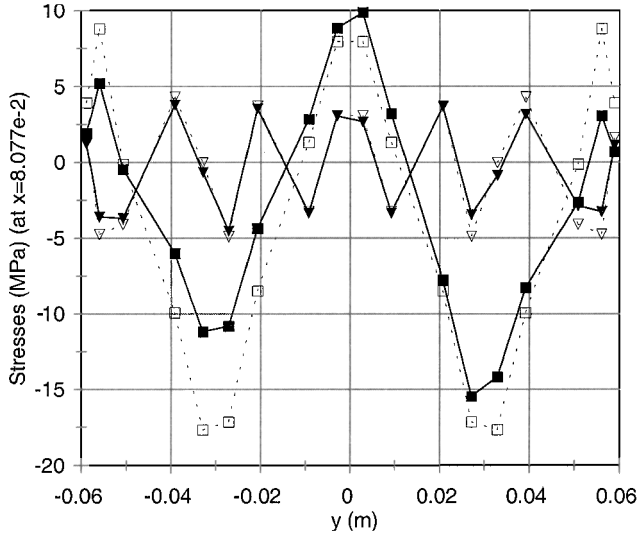

Fig. 9 Reduction of a transverse and in-plane shear stress by the PBVD procedure (x section): ■, str xy; ▼, str yz; □, ostr xy; and ▽, ostr yz.

The in-plane shear stress τ_{xy} and one of the transverse shear stresses τ_{yz} are plotted in Fig. 7 at $y = -3.923e{-}2$ m. Although the transverse shear stress may be smaller in magnitude compared to the other stresses, it is clearly not negligible. This justifies the need to use a displacement field, such as the present one, that is able to capture the transverse shear effects. From Fig. 7, it can be seen that at points with high-stress magnitudes, applying PBVD would reduce their magnitudes significantly. This effect is consistent with the PBVD algorithm, which was founded on the premise of reducing the worst local effects.

The normal in-plane stresses at the perpendicular cross section, $x = 8.077e{-}2$ m is plotted in Fig. 8, whereas the transverse and in-plane shear stresses are found in Fig. 9. This cross section is almost at the center of the cantilever plate running across its width. Regions of high stresses in both Figs. 8 and 9 have been significantly reduced. For example in Fig. 8, the maximum reduction of σ_{yy} of approximately 60–45 MPa (25%) was achieved, whereas in Fig. 9, the in-plane shear (twist) stress τ_{xy} was reduced from 18 to 11 MPa (38%) at one region. Note that in all graphs the discrete nature of the stress distribution is quite evident and that this is a mere reflection of the discrete actuator patch layout of the physical structure.

Conclusions

A novel shape control algorithm that uses both displacement and slope criteria is presented. The FE formulation was based on a combination of third-order displacement field and layerwise concepts developed by the authors for laminated smart composite plate structures. Many existing shape control algorithms that are displacement based yield reasonable results. However, this paper has shown that, for an extended structure, with many independent actuators distributed across the structure, it was found that pure displacement-based shape control predicts a voltage configuration that, when applied, produces regions of bumpiness in the shape due to localized effects.

The PBVD is an iterative algorithm designed to reduce this effect by targeting some of the worst affected regions by using slope values. Regions where the desired slope differs most from the actual slope are improved first. Because the displacement and slope are conflicting criteria, the slopes would have to be improved at the expense of the displacement. This has been designed into the algorithm to enable the user to decide the extent of the worsening of the displacement criteria that is tolerable. The results have shown that the algorithm is successful in achieving its goal of determining the voltage configuration to actuate the structure to conform to the desired shape, as well as smoothing the structure to a certain extent.

In practical, real-sized structures where discrete actuators are in operation, although the bumpiness may not always be obvious, the large gradients imply large internal strains and, thus, large internal stresses. This paper has shown that the so-called smoothing that is achieved via the algorithm is not merely an aesthetic improvement. In fact, the significance of smoothing extends to alleviating unnecessary internal stresses that could be generated if a purely displacement-shape control is used.

Acknowledgments

The authors acknowledge the support of the Australian Research Council under the large grant scheme, Grant A89905990. C. Chee is a recipient of the Australian Postgraduate Award and the Aeronautical Engineering Department Supplementary Scholarship.

References

[1]Haftka, R. T., and Adelman, H. M., "Selection of Actuator Locations for Static Shape Control of Large Space Structures by Heuristic Integer Programming," *Computers and Structures*, Vol. 20, Nos. 1–3, 1985, pp. 575–585.

[2]Okubo, H., Komatsu, N., and Tsumura, T., "Tendon Control System for Active Shape Control of Flexible Space Structures," *Journal of Intelligent Material Systems and Structures*, Vol. 7, No. 4, 1996, pp. 470–475.

[3]Tabata, M., and Natori, M. C., "Active Shape Control of a Deployable Space Antenna Reflector," *Journal of Intelligent Material Systems and Structures*, Vol. 7, No. 2, 1996, pp. 235–240.

[4]Paradies, R., Hertwig, M., and Elspass, W. J., "Shape Control of an Adaptive Mirror at Different Angles of Inclination," *Journal of Intelligent Material Systems and Structures*, Vol. 7, No. 2, 1996, pp. 203–210.

[5]Donthireddy, P., and Chandrashekhara, K., "Modelling and Shape Control of Composite Bemas with Embedded Piezoelectric Actuators," *Composite Structures*, Vol. 35, No. 2, 1996, pp. 237–244.

[6]Eisenberger, M., and Abramovich, H., "Shape Control of Non-Symmetric Piezolaminated Composite Beams," *Composite Structures*, Vol. 38, Nos. 1–4, 1997, pp. 565–571.

[7]Koconis, D. B., Kollar, L. P., and Springer, G. S., "Shape Control of Composite Plates and Shells with Embedded Actuators. I. Voltages Specified," *Journal of Composite Materials*, Vol. 28, No. 5, 1994, pp. 415–458.

[8]Koconis, D. B., Kollar, L. P., and Springer, G. S., "Shape Control of Composite Plates and Shells with Embedded Actuators. II. Desired Shape Specified," *Journal of Composite Materials*, Vol. 28, No. 3, 1994, pp. 262–285.

[9]Hsu, C. Y., Lin, C. C., and Gaul, L., "Shape Control of Composite Plates by Bonded Actuators with High Performance Configuration," *Journal of Reinforced Plastics and Composites*, Vol. 16, No. 18, 1997, pp. 1692–1710.

[10]Chandrashekhara, K., and Varadarajan, S., "Adaptive Shape Control of Composite Beams with Piezoelectric Actuators," *Journal of Intelligent Material Systems and Structures*, Vol. 8, No. 2, 1997, pp. 112–124.

[11]Reddy, J. N., "A Simple Higher Order Theory for Laminated Composite Plates," *Journal of Applied Mechanics*, Vol. 51, No. 4, 1984, pp. 745–752.

[12]Varadarajan, S., Chandrashekhara, K., and Agarwal, S., "Adaptive Shape Control of Laminated Composite Plates Using Piezoelectric Materials," *AIAA Journal*, Vol. 36, No. 9, 1998, pp. 1694–1698.

[13]Balakrishnan, A. V., "Shape Control of Plates with Piezo Actuators and Collocated Position/Rate Sensors," *Applied Mathematics and Computation*, Vol. 63, No. 2–3, 1994, pp. 213–234.

[14]Tan, Z., and Bainum, P. M., "Optimal Linear Quadratic Gaussian Digital Control of an Orbiting Tethered Antenna/Reflector System," *Journal of Guidance, Control, and Dynamics*, Vol. 17, No. 2, 1994, pp. 234–241.

[15]Tan, Z., and Bainum, P. M., "The Hybrid Control of an Orbiting Tethered Antenna/Reflector System," *Journal of the Astronautical Sciences*, Vol. 42, No. 3, 1994, pp. 343–359.

[16]Subramanian, G., and Mohan, P., "A Fast Algorithm for the Static Shape Control of Flexible Structures," *Computers and Structures*, Vol. 59, No. 3, 1996, pp. 485–488.

[17]Chee, C., Tong, L., and Steven, G., "A Mixed Model for Adaptive Composite Plates with Piezoelectric for Anisotropic Actuation," *Computers and Structures*, Vol. 77, No. 3, 2000, pp. 253–268.

[18]Chee, C., Tong, L., and Steven, G., "A Buildup Voltage Distribution (BVD) Algorithm for Shape Control of Smart Plate Structures," *Computational Mechanics*, Vol. 26, No. 2, 2000, pp. 115–128.

[19]Lo, K. H., Christensen, R. M., and Wu, E. M., "A High Order Theory of Plate Deformation—Part 1 and 2: Homogeneous Plates," *Journal of Applied Mechanics*, Vol. 44, 1977, pp. 663–676.

[20]Saravanos, D. A., and Heyliger, P. R., "Coupled Layerwise Analysis of Composite Beams with Embedded Piezoelectric Sensors and Actuators," *Journal of Intelligent Material Systems and Structures*, Vol. 6, No. 3, 1995, pp. 350–363.

[21]Robbins, D. H., and Reddy, J. N., "Analysis of Piezoelectrically Actuated Beams Using a Layer-Wise Displacement Theory," *Computers and Structures*, Vol. 41, No. 2, 1991, pp. 265–279.

[22]Tiersten, H. F., *Linear Piezoelectric Plate Vibrations—Elements of the Linear Theory of Piezoelectricity and the Vibrations of Piezoelectric Plates*, Plenum, New York, 1969, Chap. 5.

A. Chattopadhyay
Associate Editor